RESEARCH ARTICLE
doi: 10.2306/scienceasia1513-1874.2022.122

*ScienceAsia* 48 (2022): **847–854**

# Facile and green synthesis of AgNPs by microwave-assisted method using curcumin biomaterial for improving antibacterial activities of NR/Ag composite sheets

**Warot Chotpatiwetchkul**[a], **Monthol Saengsawang**[a], **Chaval Sriwong**[a,b,*]

[a] Department of Chemistry, School of Science, King Mongkut's Institute of Technology Ladkrabang, Bangkok 10520 Thailand

[b] Center of Excellence in Smart Materials Research and Innovation, King Mongkut's Institute of Technology Ladkrabang, Bangkok 10520 Thailand

[*]Corresponding author, e-mail: chaval.sr@kmitl.ac.th

*Received 14 Nov 2021, Accepted 15 Jun 2022*
*Available online 21 Aug 2022*

**ABSTRACT**: Natural rubber (NR)-based composites or hybrid products obtained from NR and several nano-materials are of interest due to their wide range of applications. However, they are easily contaminated with bacteria or fungi that can affect human health, especially those used in food container and on human skin. Herein, we present the composite sheets of NR latex and silver nanoparticles (AgNPs) with exceptionally high antibacterial activities. AgNPs were firstly synthesized by a facile, rapid, and green microwave-assisted method using curcumin as a biomaterial reductant and stabilizer. Then, natural rubbers loaded with AgNPs (NR/Ag) composite sheets were prepared via a simple direct latex mixing-casting process of NR latex and various contents of AgNPs. The result demonstrated that the synthesized AgNPs had a spherical-like shape of $12.25 \pm 3.13$ nm. All the prepared NR/Ag composite sheets exhibited high performance in antibacterial properties against *Staphylococcus aureus* and *Escherichia coli*, and the antibacterial activities were dependent on the loaded AgNPs content. In this study, it is anticipated that these rapid, simple, green, and effective methods can suitably be scaled up for large-scale preparation of the stabilized AgNPs colloid and NR/Ag composite products.

**KEYWORDS**: silver nanoparticles (AgNPs), curcumin, microwave-assisted method, natural rubber composite sheet, antibacterial activity

## INTRODUCTION

Natural rubber (NR) is a natural elastic polymer consisting of cis-1,4-polyisoprene. It has been widely used in many industrial applications (such as tires, sports articles, sealing materials, health care products, and dairy rubber items [1, 2]) due to its non-toxic, high tensile strength, good elasticity, toughness, and low heat hysteresis [3]. However, the NR raw-materials and NR products are easily contaminated with any bacteria or fungi that can affect human health, especially those NR products used in food container and on human skin [4]. Thus, many researchers and industrial developers have been interested in improving the antibacterial NR.

NR-based composites or hybrid products incorporated with several nano-materials have attracted much attention for the last few decades due to their wide range of applications [1, 4–8]. In general, various methods have been used for preparing the NR-based composite materials, for instance, melt bending, solution mixing, in-situ polymerization, ball milling, and foaming processes [9, 10]. Nevertheless, some of these methods are complicated with inconvenient process and several disadvantages [10]. Therefore, a simple, low cost, suitable, and large-scale process for NR-based composite production has been a real interesting challenge to many researchers including us.

Amongst nano-materials, silver nanoparticles (AgNPs) have tremendous applications in many fields: sensors, optics, catalysts, electronics, clothing, biomedical, and antimicrobial agents [11–16]. Although a chemical reduction is the most popular method for the synthesis of AgNPs by using reducing agents, such as citric acid, dimethylformamide, hydrazine, and sodium borohydride, these reducing chemicals are toxic and cause environmental problems [11, 13]. Alternatively, plant-derived natural chemicals, e.g., AgNPs, have been used as reducing and stabilizing agents in metal nanoparticle syntheses, and they are considered greener and possibly more cost-effective processes [17–21].

Curcumin is a green biomaterial and belongs to curcuminoids. It is obtained by extraction from dried roots of *Curcuma longa* (*C. longa*), commonly called turmeric. Curcumin has been used as a green reductant and stabilizer for the synthesis of AgNPs without additional chemicals [20–23]. Compared with the traditional heating process, microwave-assisted synthesis was a more promising method for metal nanoparticles' preparation because it was a rapid, simple, green, and effective process. Moreover, the microwave-assisted synthesis created uniform nanoparticles with higher degree of crystallinity and provided greater control

over the shape and morphology of the nanostructures produced [24, 25]. However, to the best of our knowledge, there have been no reports on the microwave-assisted green synthesis of AgNPs by using a natural curcumin biomaterial as both reducing and stabilizing agent.

In the present work, we present the synthesis of AgNPs colloid through a facile, rapid and green microwave-assisted method using curcumin as reducing, capping and stabilizing agent. Then, the composite sheets of NR loaded with AgNPs (NR/Ag) were prepared via a simple direct mixing-casting process of NR latex with various AgNPs contents. All synthesized samples were characterized and confirmed by several techniques. Moreover, the antibacterial properties of the pristine NR and all the prepared NR/Ag composite sheets were tested against *S. aureus* and *E. coli* bacteria. Besides, SEM morphologies of both bacteria in inhibition and growth zones were also investigated. Interestingly, this study demonstrates that the curcumin biomolecules are not only used as both reductant and stabilizer for synthesizing AgNPs, but it also acted as dispersant, enhancing the well-dispersion and incorporation of as-synthesized AgNPs into the NR matrix of the composite sheets.

## MATERIALS AND METHODS

### Chemicals and materials

Silver nitrate ($AgNO_3$ > 99% purity) and ammonia solution ($NH_3$, 28–30%) were purchased from Merck, Germany. Curcumin powder (> 99.5% purity) was supplied from Ouay un Osoth Co., Ltd., Thailand. Natural rubber latex (NRL, 60% dry rubber content, high ammonia) was obtained from Chana Latex Co., Ltd., Thailand. Microwave oven Model MG23F301 was from Samsung Thailand. Petri dish mould (3.5-inch diameter) was obtained from PYREX, USA.

### Preparation of curcumin solution

About 50 mg of curcumin powder was added into 100 ml of deionized (DI) water and then heated at 55–60 °C for 15 min. After that, the curcumin solution was filtered to separate the undissolved curcumin powder, and the solution was diluted by DI water (at a concentration of 0.10 mg/ml) to obtain a light-yellow curcumin solution to be used in further experiments.

### Synthesis of silver nanoparticles (AgNPs)

The colloidal AgNPs sample was synthesized by a facile, rapid, and green microwave-assisted method using curcumin as a reductant and stabilizer. In this typical procedure, 0.20 g of $AgNO_3$ was dissolved in 10 ml of distilled water, mixed with 20 ml of the prepared curcumin solution and then stirred for 3 min. Next, the mixture was irradiated by microwave oven at the power of 350 W for 180 s with pauses every 15 s to cool down the mixture. During the irradiation, the mixture's color changed from light-yellow to yellow and then orange-brown, confirming the formation of AgNPs colloid. Finally, the as-synthesized AgNPs colloid with the concentration of 21.5 mg/ml was obtained.

### Preparation of NR/Ag composite sheets

The NR/Ag composite sheets were easily prepared by a simple direct latex mixing-casting method using NR latex (60%, HA) with various contents of colloidal AgNPs loading (1, 2 and 3 ml). In a typical procedure, 1 ml of the colloidal AgNPs (21.5 mg/ml) was mixed with 0.3 ml of $NH_3$ solutions and stirred for 3 min. Then, the mixture was added into 7 ml of NR latex and stirred for another 10 min. After that, the mixture was casted into petri dish mould and left to dry at room temperature for 13–14 h, resulting in NR/Ag-1 composite sheet sample. To investigate the effect of AgNPs loading contents, NR/Ag-2 and NR/Ag-3 composite sheets were also prepared similarly to the aforementioned method using 2 ml and 3 ml of AgNPs colloids, respectively.

### Characterization of synthesized AgNPs colloid

The phase structures of the pristine NR and all NR/Ag composite sheets were identified by X-ray diffraction (XRD) (XRD-6100, Shimadzu, Japan). The absorption of synthesized AgNPs colloid was analyzed by UV-visible spectroscopy (Evolution 201, Thermo Fisher Scientific Inc., USA). The particles sizes and shapes of colloidal AgNPs were also examined by transmission electron microscopy (TEM) (JEOL-2100, Japan) attached with selected area electron diffraction (SAED) techniques. The chemical functional groups of NR and NR/Ag composite sheets were confirmed using a reflection Fourier-transformed infrared spectroscopy (FT-IR) (Nicolet iS50, Thermo Fisher Scientific Inc.). Raman spectroscopy was performed using DXR Smart (Thermo Fisher Scientific Inc.) equipped with a 532 nm laser excitation. The surface morphologies of the pristine NR and NR/Ag composite sheets were studied by scanning electron microscopy (SEM) (JEOL-JSM5800LV, Japan) attached with energy dispersive X-ray spectrometer (EDS) (Oxford ISIS 300).

### Antibacterial property tests

The antibacterial properties of the pristine NR and all NR/Ag composite sheets were tested by an agar disk-diffusion method similar to what described in a previous paper [26], against the Gram-positive *S. aureus* and the Gram-negative *E. coli*. All sheet samples were cut into $10 \times 10$ mm$^2$ squares. The composite sheet samples were incubated at 37 °C for 24 h in an incubation chamber. Then, the inhibition zones developed on the sheets were photographed and reported.

## RESULTS AND DISCUSSION

### Synthesis concept of colloidal AgNPs

A proposed schematic mechanism of colloidal AgNPs formation process by rapid microwave-assisted method using curcumin bio-material as reductant and stabilizer was illustrated (Fig. 1). When the curcumin and the $AgNO_3$ solutions were mixed, (a) curcumin biomolecules directly reacted with silver(I) ions ($Ag^+$) to form chelated compound by coordinate bond and electrostatic attraction force between the lone pair electron donor from oxygen atoms of phenolic diketone of curcumin and $Ag^+$ ions [20, 23]. During microwave irradiation, several $Ag^0$ nucleation due to curcumin reductant and stabilizer were firstly generated (b)–(c), leading to the aggregation (Ostwald ripening) of $Ag^0$ nucleation, (d) forming stabilized AgNPs [24]. The color of the mixture solution was changed from light-yellow to orange-brown after microwave irradiation for 180 s. This result concluded that curcumin could promote the formation and stabilization of spherical-like shape AgNPs colloid over a facile, rapid, and green microwave-assisted method.

### Characterization of synthesized AgNPs colloid

The formation of AgNPs by a rapid, simple, and green microwave-assisted process was evaluated by UV-Vis and TEM techniques, and the results were displayed in Fig. 2a and 2b, respectively. The colloidal AgNPs characteristic peak was clearly seen at around 425 nm (Fig. 2a) due to the surface plasmon resonance (SPR) behaviour of $AgNO_3$ and curcumin in the mixture [13, 19, 23, 25]. The result could indicate that $Ag^+$ precursors are reduced and aggregated to AgNPs, and curcumin presumably acts as a reductant, as reported in the previous studies [20, 23]. It is worth noted that the absorption intensities of the SPR peaks of synthesized AgNPs were increased with the increases of irradiation times, implying that more AgNPs could be generated with prolonged irradiation time [17, 18]. However, when the irradiation time was longer than 180 s (i.e., left overnight at room temperature), an unstable colloid with self-agglomeration of AgNPs could be observed. This result was caused by the destruction of curcumin molecules (as a stabilizer) due to the over-heat of colloidal AgNPs media under long time irradiation.

Fig. 2b displays the TEM image of the synthesized colloidal AgNPs, showing spherical-like shape of about $12.25 \pm 3.13$ nm in diameter and with high intersperse. The size distribution and the mean size of the AgNPs were shown in Fig. 2c. Moreover, the crystal structure of AgNPs was well-confirmed by selected area electron diffraction (SAED), as presented in Fig. 2d. The rings patterns corresponded to the plane families 111, 200, 220, and 311 of the face-centered-cubic (fcc) silver structure [25]. Also, the silver (Ag) element of as synthesized AgNPs was clearly confirmed by EDS spectrum and EDS mapping (Fig. S1). In addition, Fig. 2e clearly shows the physical appearance of the yellow-brown NR/Ag composite sheet.

### Characterizations of NR/Ag composite sheets

The FTIR spectra of the pristine NR sheet and the NR/Ag composite sheets were shown in Fig. 3. Absorption peaks of the NR/Ag composite sheets (Fig. 3b and 3c) were: 3270 $cm^{-1}$ for —OH stretching, 2935–2850 $cm^{-1}$ for —C=$CH_2$, $CH_3$ stretching, 1648 $cm^{-1}$ for —C=C— stretching of isoprene group, 1440 $cm^{-1}$ for —$CH_2$ deformation, 819 $cm^{-1}$ for =C-H out of plane bending, and 569 $cm^{-1}$ for —C-C-C— main chain deformation [27, 28], well-corresponding to the pristine NR sheet (Fig. 3a). This result implied that the chemical structure of natural rubber was not changed or decomposed by the loaded AgNPs in the natural rubber matrix.

The Raman spectra of the pristine NR and the NR/Ag composite sheets were shown (Fig. 4). Compared with the pristine NR sheet (Fig. 4a), all the absorption peaks intensities for natural rubber molecule, especially the isoprene, —C=C— (at around 1650 $cm^{-1}$) [29, 30], of the composite sheets (in Fig. 4b and 4c) were obviously decreased with the increases of AgNPs loading, suggesting more incorporated AgNPs in the NR matrix. The absorption peaks of NR/Ag-3 sheet (Fig. 4c) had the lowest intensities due to the highest content of AgNPs loaded into the NR matrix. The result could be due to the highest loading of AgNPs into the NR matrix contributing to the highest number of defected NR molecules (especially —C=C— isoprene group) and the defected NR chain. Hence, the Raman intensities of the NR/Ag composite sheets were decreased with the increases of AgNPs loading in comparison to the pristine NR sample. This result was in agreement with the SEM and EDS mapping images, as shown in Fig. 5b, 5c; and Fig. 6d, 6f, respectively, AgNPs had well-incorporated and dispersed into the NR matrix.

The XRD patterns of the pristine NR sheet and the NR sheets loaded with different contents of colloidal were shown in Fig. S2. A strong diffraction peak at 2θ around 19.0° corresponding to NR amorphous structure was observed in the pristine NR and all the NR/Ag composite sheets [31, 32]. Notably, the peak intensity of NR/Ag-3 sheet was decreased, and a broader peak could be observed as well. These results were due to the incorporation and dispersion of AgNPs into the NR matrix. However, a major diffraction peak at 2θ around 38.1° [33, 34] of AgNPs was not detected; probably, because a very small amount of AgNPs was loaded into the NR/Ag composite sheets.

The SEM cross-sections of the pristine NR sheet and the NR/Ag composite sheets were displayed in Fig. 5. The morphologies of the pristine NR showed

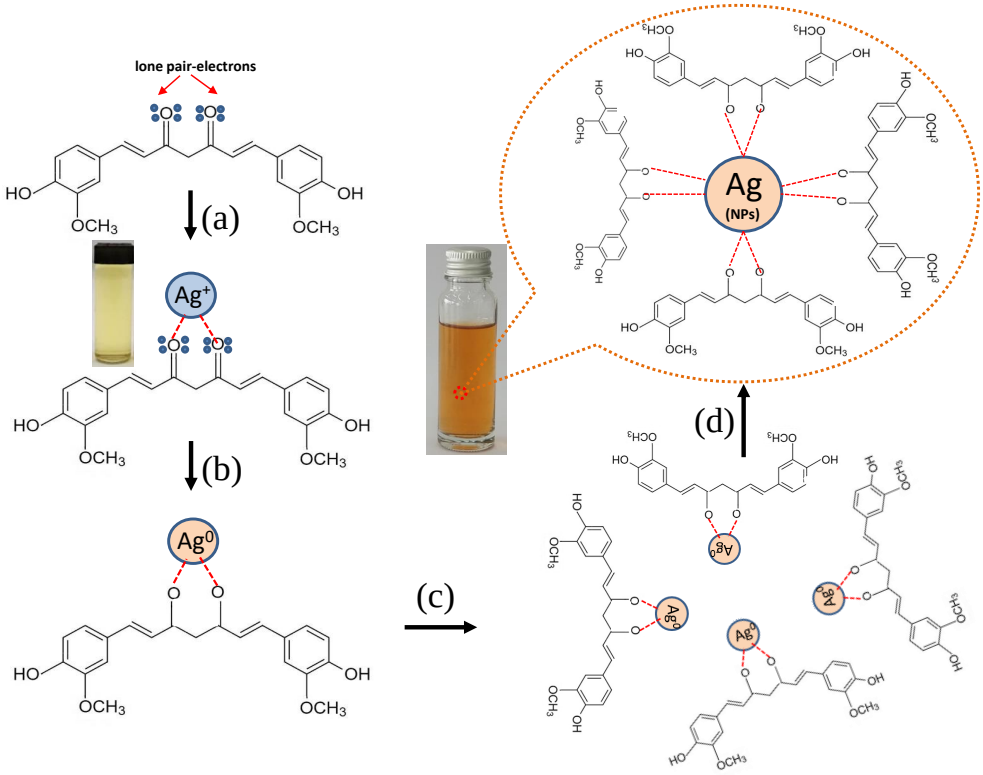


**Fig. 1** Proposed schematic mechanism of colloidal AgNPs formation process by rapid, green microwave-assisted method using curcumin as biomaterial reductant, capping and stabilizer.

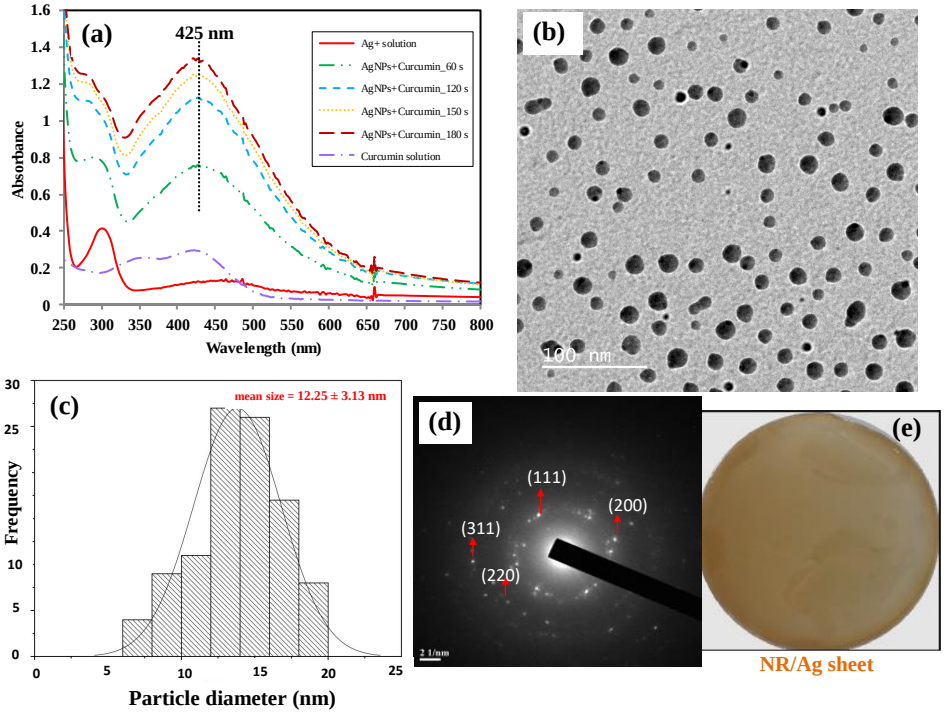


**Fig. 2** (a), UV-Vis spectra; (b), TEM image; (c), size distribution; (d), SAED image of the colloidal AgNPs irradiated at 350 W for 180 s; and (d), photograph of NR/Ag composite sheet.

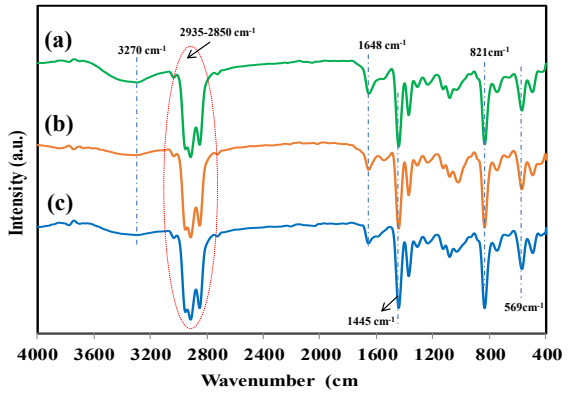


**Fig. 3** ATR-FTIR spectra of: (a), pristine NR sheet; (b), NR/Ag-1 composite sheet; and (c), NR/Ag-3 composite sheet.

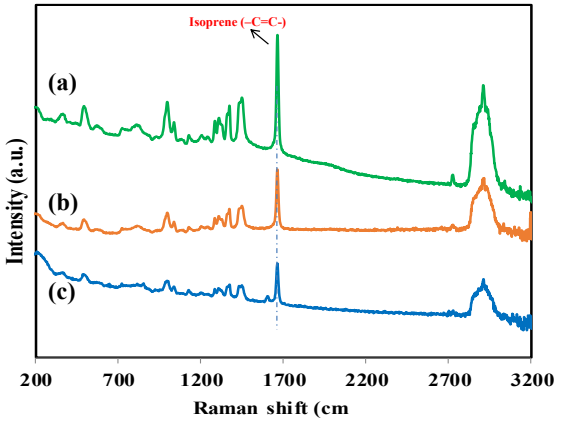


**Fig. 4** Raman spectra of: (a), pristine NR sheet; (b), NR/Ag-1 composite sheet; and (c), NR/Ag-3 composite sheet.

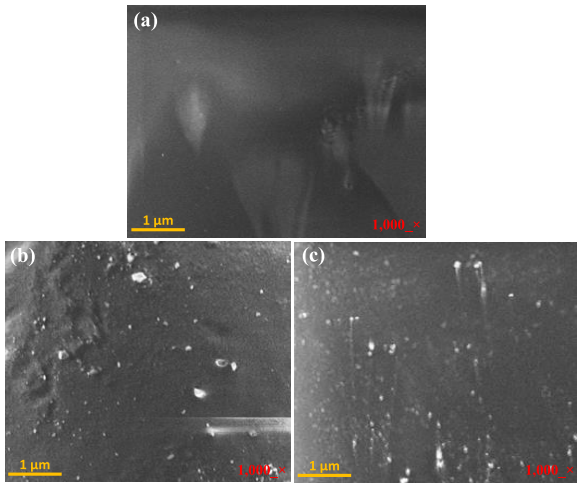


**Fig. 5** SEM cross-section images of: (a), pristine NR sheet; (b), NR/Ag-1 composite sheet; and (c), NR/Ag-3 composite sheet.

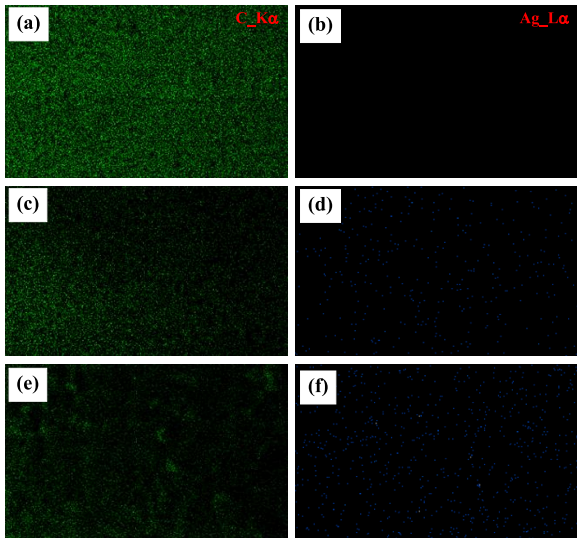


**Fig. 6** EDS mapping of: (a)–(b), pristine NR sheet; (c)–(d), NR/Ag-1 composite sheet; and (e)–(f), NR/Ag-3 composite sheet.

a very smooth surface (Fig. 5a), whereas the NR/Ag composite sheets had a rough surface that increased with the increases of AgNPs loading contents (Fig. 5b and 5c).

To confirm the dispersion and the incorporation of AgNPs into the NR matrix, the EDS mapping of pristine NR and the NR/Ag sheet samples were examined, and the results were presented in Fig. 6. Compared with the pristine NR sheet (Fig. 5a, the NR/Ag composite sheets (Fig. 5b and 5c) had more blue light-spots of Ag atoms in the NR matrix with increasing AgNPs loading. The light-spots were well-dispersed, incorporated, and impregnated into the matrix of NR sheets of NR/Ag-1 (Fig. 6b) and NR/Ag-3 (Fig. 6b). The result indicated that the curcumin biomolecules were not only used as reducing, capping, and stabilizing agent; but it also acted as dispersant, enhancing the well-dispersion and incorporation of AgNPs into the NR matrix. In addition, the presence of C and Ag atoms in the pristine NR and the NR/Ag sheets were analysed, and the results were showed in Fig. S3a and S3b, respectively. The EDS spectrum clearly confirmed the existence of Ag element in the NR/Ag composite sheet (Fig. S3b) [35, 36].

### Antibacterial activities of NR/Ag composite sheets

To investigate the application of the synthesized colloidal AgNPs, the NR was mixed with different loadings of AgNPs to prepare the NR/Ag composite sheets. The antibacterial activities of the NR/Ag composite sheets were displayed in Fig. 7. Compared with the

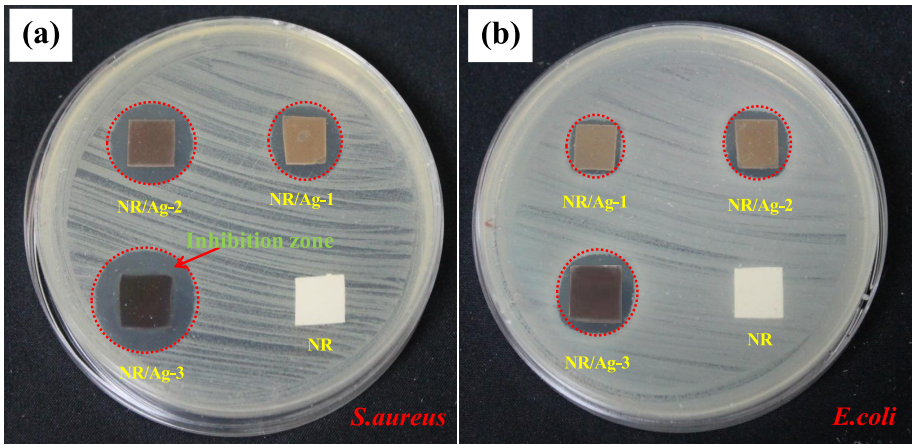


**Fig. 7** Antibacterial activities of pristine NR and all the NR/Ag composite sheets against: (a), *S. aureus*; and (b), *E. coli*.

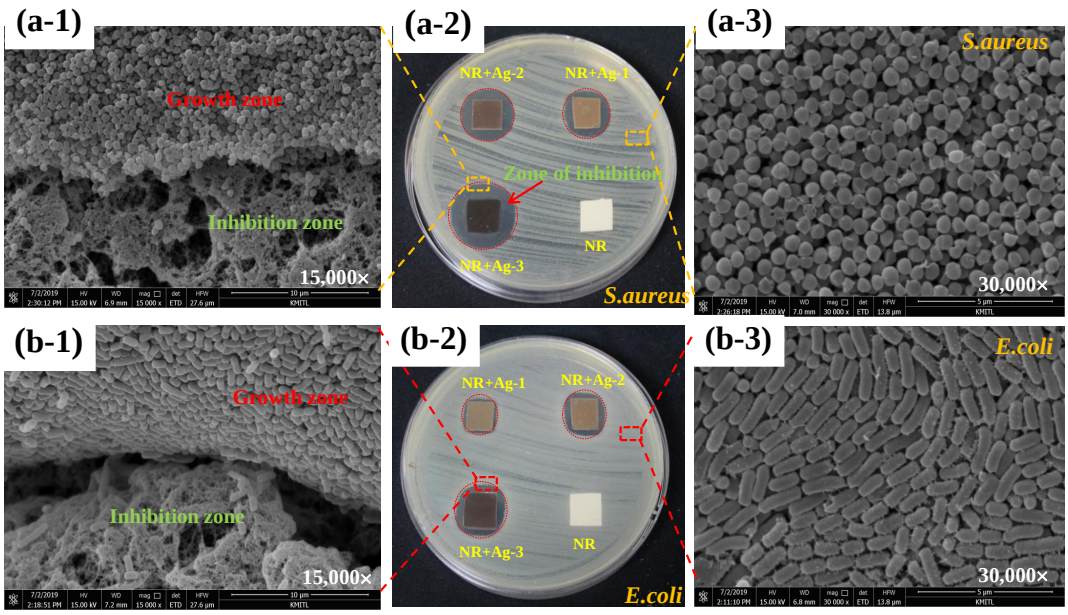


**Fig. 8** SEM micrographs of inhibition zones and growth zones of: (a), *S. aureus*; and (b), *E. coli* over the NR/Ag-3 composite sheet.

pristine NR sheet, the NR/Ag composite sheets had excellent antibacterial activities against both *S. aureus* and *E. coli*, as shown in Fig. 7a and 7b, respectively. These results implied that the antibacterial properties of the NR/Ag composite sheets could be attributed to the presence of AgNPs [17, 21, 22]. In comparison, the NR/Ag-3 composite sheet revealed the highest zones of inhibition against both bacteria (red arrow, Fig. 7a; and red circle, Fig. 7b), whereas no inhibition against both bacteria was observed for the pristine NR sheet. The inhibition zones for NR/Ag composite sheets against both bacteria increased with increases of loaded AgNPs content, which was consistent with the trend of increasing AgNPs content, resulting in increasing bacteria inhibition zones [22, 33, 35, 37]. The inhibition zone diameters of all the composite

**Table 1** Average inhibition zones of the prepared NR/Ag composite sheets against *S. aureus* and *E. coli*.

| Sample sheet | Inhibition zone diameter (mm) | |
|---|---|---|
| | *S. aureus* | *E. coli* |
| pristine NR | inactive | inactive |
| NR/Ag-1 | 14.1 ± 0.1 | 11.6 ± 0.3 |
| NR/Ag-2 | 17.4 ± 0.3 | 13.3 ± 0.3 |
| NR/Ag-3 | 21.3 ± 0.4 | 16.5 ± 0.2 |

sheets were shown in Table 1. It was noticed that gram-negative *E. coli* (Fig. 7b) exhibited smaller zones of inhibitions than gram-positive *S. aureus* (Fig. 7a). The result might be due to the fact that *E. coli* has a thicker cell wall covered with an outer membrane. Hence, *E. coli* showed a stronger resistance against AgNPs attack than *S. aureus*, which is consistent with previous studies [21, 38].

In addition, the morphologies of both *E. coli* and *S. aureus* over the NR/Ag composite sheets were investigated by SEM technique (Fig. 8). Fig. 8(a-3) shows *S. aureus* with a spherical-shaped structure, whereas *E. coli* had rod-shaped structure (Fig. 8(b-3)). After incubation at 37 °C for 24 h, the inhibition zones of *S. aureus* (in Fig. 7a) and *E. coli* (in Fig. 7b) over the NR/Ag composite sheets were clearly observed. As can be seen from the inhibition zones in Fig. 8, the membranes and cells of both bacteria were damaged, and not survived on an agar gel dish [39, 40]. The result clearly confirmed both bacteria were dead, and growth was stopped by the NR/Ag composite sheets. This may be due to the AgNPs with a size range of 1–10 nm [20], and $Ag^+$ ions from NR/Ag surface which can be released and directly attached to bacterial cell membrane as well as the membrane permeability [37, 41]. Thus, the generated ROS put stress on the bacterial membrane and affect cell division, respiration, and ultimately the survival of the cell, resulting in bacterial membrane damages and cell deaths [37, 41, 42].

## CONCLUSION

In summary, the colloidal AgNPs were successfully synthesized by a microwave-assisted method using curcumin biomaterial as a reducing, capping, and stabilizing agent. The NR/Ag composite sheets were prepared by a direct latex mixing-casting method using NR latex (60%, HA) and AgNPs colloid. These methods are simple, very fast, low cost, green, scalable, and effective. All the NR/Ag composite sheets exhibited high performance in antibacterial activities against both gram-positive *S. aureus* and gram-negative *E. coli*, and the activities positively depended on the AgNPs loading contents. The highest antibacterial activity was clearly observed in the NR/Ag-3 composite sheet. Scaling up for a large-scale production of both the stabilized AgNPs colloid and the NR/Ag composite sheets is foreseen for future use.

## Appendix A. Supplementary data

Supplementary data associated with this article can be found at http://dx.doi.org/10.2306/scienceasia1513-1874.2022.122.

*Acknowledgements*: This work was supported by the School of Science, King Mongkut's Institute of Technology Ladkrabang (KMITL). The research has also received funding support from the National Science, Research and Innovation Fund (NSRF). The authors would like to thank all researchers and laboratory members from the Center of Excellence in Smart Materials Research and Innovation, King Mongkut's Institute of Technology Ladkrabang for their equipment, knowledge, and technical support.

## REFERENCES

1. An D, Cheng S, Jiang C, Duan X, Yang B, Zhang Z, Li J, Liu Y, et al (2020) A novel environmentally friendly boron nitride/lignosulfonate/natural rubber composite with improved thermal conductivity. *J Mater Chem C* **8**, 4801–4809.
2. Zheng T, Zheng X, Zhan S, Zhou J, Liao S (2021) Study on the ozone aging mechanism of natural rubber. *Polym Degrd Stab* **186**, 109514.
3. Abu Bakar NHH, Ismail J, Abu Bakar M (2007) Synthesis and characterization of silver nanoparticles in natural rubber. *Mater Chem Phys* **104**, 276–283.
4. Rathnayake I, Ismail H, Azahari B, Bandara C, Rajapakse S (2013) Novel method of incorporating silver nanoparticles into natural rubber latex foam. *Polym Plast Technol Eng* **52**, 885–891.
5. Peng Z, Feng C, Luo Y, Li Y, Kong LX (2010) Self-assembled natural rubber/multi-walled carbon nanotube composites using latex compounding techniques. *Carbon* **48**, 4497–4503.
6. Yangthong H, Pichaiyut S, Jumrat S, Wisunthorn S, Nakason C (2018) Novel natural rubber composites with geopolymer filler. *Adv Polym Technol* **37**, 2651–2662.
7. Stanier DC, Patil AJ, Sriwong C, Rahatekar SS, Ciambella J (2014) The reinforcement effect of exfoliated graphene oxide nanoplatelets on the mechanical and viscoelastic properties of natural rubber. *Compos Sci Technol* **95**, 59–66.
8. Matos CF, Galembeck F, Zarbin AJG (2012) Multifunctional materials based on iron/iron oxide-filled carbon nanotubes/natural rubber composites. *Carbon* **50**, 4685–4695.
9. Harito C, Bavykin DV, Yuliarto B, Dipojono HK, Walsh FC (2019) Polymer nanocomposites having a high filler content: synthesis, structures, properties, and applications. *Nanoscale* **11**, 4653–4682.
10. Khatoon H, Ahmad S (2017) A review on conducting polymer reinforced polyurethane composites. *J Ind Eng Chem* **53**, 1–22.
11. Yuan W, Gu Y, Li L (2012) Green synthesis of graphene/Ag nanocomposites. *Appl Surf Sci* **261**, 753–758.
12. Wang LS, Wang CY, Yang CH, Hsieh CL, Chen SY, Shen CY, Wang JJ, Huang KS (2015) Synthesis and antifungal effect of silver nanoparticles-chitosan composite particles. *Int J Nanomedicine* **10**, 2685–2696.

13. Krainoi A, Kummerlöwe C, Nakaramontri Y, Wisunthorn S, Vennemann N, Pichaiyut S, Kiatkamjornwong S, Nakason C (2019) Novel natural rubber composites based on silver nanoparticles and carbon nanotubes hybrid filler. *Polym Compos* **41**, 443–458.
14. Anancharoenwong E, Chueangchayaphan W, Rakkapao N, Marthosa S, Chaisrikhwun B (2021) Thermomechanical and antimicrobial properties of natural rubber-based polyurethane nanocomposites for biomedical applications. *Polym Bull* **78**, 833–848.
15. Khan M, Shaik MR, Adil SF, Khan ST, Warthan AA, Siddiqui MRH, Tahir MN, Tremel W (2018) Plant extracts as green reductants for the synthesis of silver nanoparticles: lessons from chemical synthesis. *Dalton Trans* **47**, 11988–12010.
16. Siraj M, Shah ZA, Ullah S, Bibi H, Suleman M, Zia A, Masood T, Iqbal Z, et al (2020) Biosynthesized silver nanoparticles from shoot and seed extracts of *Asphodelus tenufolius* for heavy metal sensing. *ScienceAsia* **46**, 697–705.
17. Ashraf H, Anjum T, Riaz S, Naseem S (2020) Microwave-assisted green synthesis and characterization of silver nanoparticles using melia azedarach for the management of fusarium wilt in tomato. *Front Microbiol* **11**, 238.
18. Yilmaz M, Turkdemir H, Akif Kilic M, Bayram E, Ciceke A, Mete A, Ulug B (2011) Biosynthesis of silver nanoparticles using leaves of Stevia rebaudiana. *Mater Chem Phys* **130**, 1195–1202.
19. Nadagouda MN, Iyanna N, Lalley J, Han C, Dionysiou DD, Varma RS (2014) Synthesis of silver and gold nanoparticles using antioxidants from blackberry, blueberry, pomegranate, and turmeric extracts. *ACS Sustain Chem Eng* **2**, 1717–1723.
20. Alsammarraie FK, Wang W, Zhou P, Mustapha A, Lin M (2018) Green synthesis of silver nanoparticles using turmeric extracts and investigation of their antibacterial activities. *Colloids Surf B* **171**, 398–405.
21. Siddiqi KS, Husen A, Rao RAK (2018) A review on biosynthesis of silver nanoparticles and their biocidal Properties. *J Nanobiotechnol* **16**, 1–28.
22. Sathishkumar M, Sneha K, Yun YS (2010) Immobilization of silver nanoparticles synthesized using *Curcuma longa* tuber powder and extract on cotton cloth for bactericidal activity. *Bioresou Technol* **101**, 7958–7965.
23. Sankar R, Rahman PK, Varunkumar K, Anusha C, Laiaiarasi A, Shivashangari KS, Ravikumar V (2017) Facile synthesis of *Curcuma longa* tuber powder engineered metal nanoparticles fo bioimaging applications. *J Mol Struct* **1129**, 8–16.
24. Ei-Naggar ME, Shaheen TI, Fouda MMG, Hebeish AA (2016) Eco-friendly microwave-assisted green and rapid synthesis of well-stabilized gold and core-shell silver-gold nanoparticles. *Carbohydr Polym* **136**, 1128–1136.
25. Kahrilas GA, Wally LM, Fredrick SJ, Hiskey M, Prieto AL, Owens JE (2014) Microwave-assisted green synthesis of silver nanoparticles using orange peel extract. *ACS Sustain Chem Eng* **2**, 367–376.
26. Rathnayake WGIU, Ismail H, Baharin A, Darsanasiri AGND, Rajapakse S (2012) Synthesis and characterization of nano silver based natural rubber latex foam for imparting antibacterial and anti-fungal properties. *Polym Test* **31**, 586–592.
27. Guidelli EJ, Ramos AP, Zaniquelli MED, Baffa O (2011) Green synthesis of colloidal silver nanoparticles using natural rubber latex extracted from Hevea brasiliensis. *Spectrochim Acta A* Spectrochim Acta A, 140–145.
28. Xu L, Huang C, Luo M, Qu W, Liu H, Gu Z, Jing L, Huang G, et al (2015) A rheological study on non-rubber component network in natural rubber. *RSC Adv* **5**, 91742–91750.
29. Bolados HA, Contreras-Cid A, Carrillo AN, Manchado ML, Pedram MY (2019) Removal of surfactant from nanocomposites films based on thermally reduced graphene oxide and natural rubber. *J Compos Sci* **3**, 31.
30. Prasertsri S, Lagarde F, Rattanasom N, Sirisinha C, Daniel P (2013) Raman spectroscopy and thermal analysis of gum and silica-filled NR/SBR blends prepared from latex system. *Polym Test* **32**, 852–861.
31. Sriwong C, Choojun K, Sriwong S (2019) High photocatalytic performance of 3D porous-structured TiO2@natural rubber hybrid sheet on the removal of indigo carmine dye in water. *SN Appl Sci* **1**, 864.
32. Sriwong C, Wongnawa S, Patarapaiboolchai O (2012) Recyclable thin TiO2-embedded rubber sheet and dye degradation. *Chem Eng J* **191**, 210–217.
33. Anandalakshmi K, Venugobal J, Ramasamy V (2016) Characterization of silver nanoparticles by green synthesis method using Pedalium murex leaf extract and their antibacterial activity. *Appl Nanosci* **6**, 399–408.
34. Khan Z, Obaid AY (2016) Seedless, copper-induced synthesis of stable Ag/Cu bimetallic nanoparticles and their optical properties. *RSC Adv* **6**, 29116.
35. Rezazadeh NH, Buazar F, Matroodi S (2020) Synergistic effects of combinatorial chitosan and polyphenol biomolecules on enhanced antibacterial activity of biofunctionalaized silver nanoparticles. *Sci Rep* **10**, 19615.
36. Verma SK, Jha E, Sahoo B, Panda PK, Thirumurugan A, Parashar SKS, Suar M (2017) Mechanistic insight into the rapid one-step facile biofabrication of antibacterial silver nanoparticles from bacterial release and their biogenicity and concentration-dependent *in vitro* cytotoxicity to colon cells. *RSC Adv* **7**, 40034.
37. Loo YY, Rukayadi Y, Nor-Khaizura MA, Kuan CH, Chieng BW, Nishibuchi M, Radu S (2018) *In vitro* antimicrobial activity of green synthesized silver nanoparticles against selected gram-negative foodborne pathogens. *Front Microbiol* **9**, 1555.
38. Raghavendra GM, Jayaramudu T, Varaprasad K, Ramesh S, Raju KM (2014) Microbial resistant nanocurcumin-gelatin-cellulose fibers for advanced medical applications. *RSC Adv* **4**, 3494.
39. Sana S, Datta S, Biswas D, Sengupta D (2018) Assessment of synergistic antibacterial activity of combined biosurfactants revealed by bacterial cell envelop damage. *Biochim Biophys Acta Biomembr* **1860**, 579–585.
40. Cui H, Zhang X, Zhou H, Zhao C, Lin L (2015) Antimicrobial activity and mechanisms of *Salvia sclarea* essential oil. *Bot Stud* **56**, 16.
41. Wang Y, Wan J, Miron RJ, Zhao Y, Zhang Y (2016) Antibacterial properties and mechanisms of gold-silver nanocages. *Nanoscale* **8**, 11143–11152.
42. Bei W, Zhou Y, Xing X, Zahi MR, Li Y, Yuan Q, Liang H (2015) Organogel-nanoemulsion containing nisin and D-limonene and its antimicrobial activity. *Front Microbiol* **6**, 1010.

## Appendix A. Supplementary data

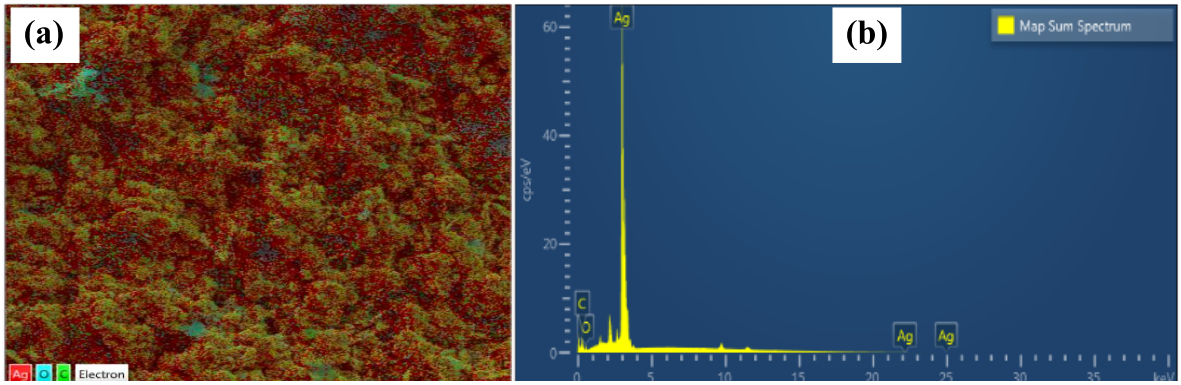


**Fig. S1** (a), EDS mapping; and (b), EDS spectrum of the synthesized AgNPs.

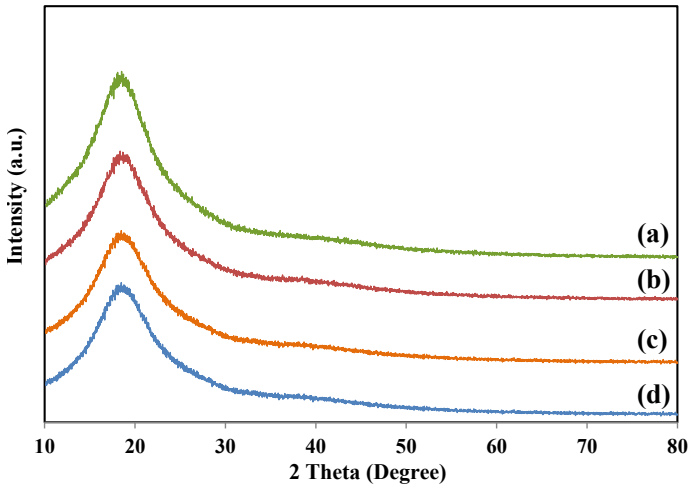


**Fig. S2** XRD patterns of: (a), pristine NR sheet; (b), NR/Ag-1 composite sheet; (c), NR/Ag-2 composite sheet; and (d), NR/Ag-3 composite sheet.

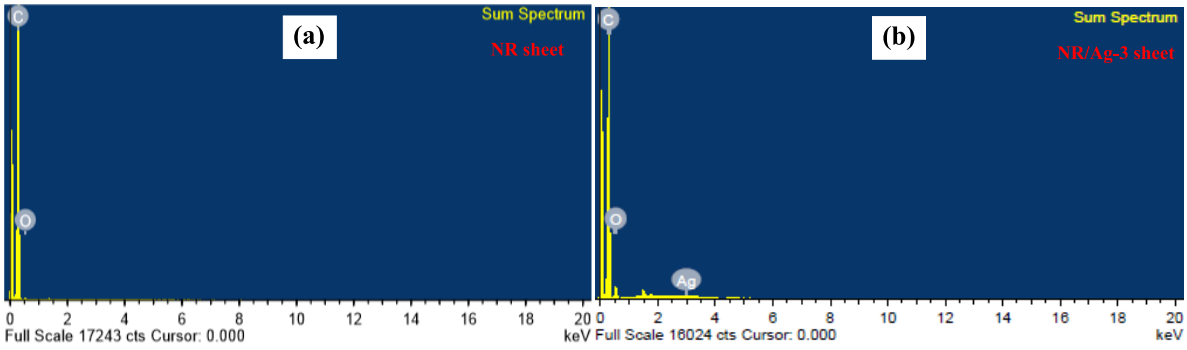


**Fig. S3** EDS spectra of: (a), pristine NR sheet; and (b), NR/Ag-3 composite sheet.